Heat transfer in Fitzhugh-Nagumo models

D. Bini
Istituto per le Applicazioni del Calcolo "M. Picone," CNR, I-00161 Rome, Italy
and International Center for Relativistic Astrophysics—ICRA, University of Rome "La Sapienza," I-00185 Rome, Italy

C. Cherubini and S. Filippi
Facoltá di Ingegneria, Università Campus Bio-Medico, Via E. Longoni 83, I-00155 Rome, Italy
and International Center for Relativistic Astrophysics—ICRA University of Rome "La Sapienza," I-00185 Rome, Italy
(Received 27 September 2005; revised manuscript received 27 June 2006; published 6 October 2006)

An extended FitzHugh-Nagumo model coupled with dynamical heat transfer in tissue, as described by a bioheat equation, is derived and confronted with experiments. The main outcome of this analysis is that traveling pulses and spiral waves of electric activity produce temperature variations on the order of tens of μ°C. In particular, the model predicts that a spiral wave's tip, heating the surrounding medium as a consequence of the Joule effect, leads to characteristic hot spots. This process could possibly be used to have a direct visualization of the tip's position by using thermal detectors.

DOI: 10.1103/PhysRevE.74.041905 PACS number(s): 87.19.Pp, 87.19.Hh

I. INTRODUCTION

The quantitative study of electrically active cells starts from the remarkable work of Hodgkin and Huxley (HH) in 1952 on nerve conduction in the squid giant axon [1–4]. These authors used extensive experimental results to derive the so-called HH model, i.e., a system of nonlinear differential equations describing the variations of membrane potential and ion conductances at a fixed point in the axon. Moreover, introducing a diffusion term, they were able to model the propagation of an action potential along the fiber and also compare it with experimental data.

The effects of temperature on the electrical activity of a nerve were first studied in 1902 [5]. It is worth mentioning the experimental work of Hodgkin and Katz [6] in 1949 on the global effects of temperature on the electrical activity of the giant axon of the squid.

The earliest clear evidence that the passage of a single nerve impulse is closely associated with membranal temperature changes was the finding of Abbott, Hill, and Hovarth [7] in 1958. Using a thermopile in conjunction with a galvanometer they performed a careful study of the time-dependent changes of temperature associated with a nerve impulse and discovered that the production of heat is followed by its reabsorption by the biological system.

Other experimental studies on the squid giant axon were performed to explore the effects of temperature on the threshold stimulating current and on the conduction velocity of the action potential [8–10], which is theoretically predicted using the HH model (see [11] and references therein). Many studies concerning mechanical and thermal changes associated with the excitation process in nerve fibers have been conducted [7,12,13]. In particular the works of Tasaki and co-workers [14,15] have shown that the thermal response starts and reaches a peak on the order of some μ°C nearly simultaneously with the electric response. As expected, the phase of heat production is followed immediately by the phase of heat absorption and no net heat release after passage of the action potential. Global temperature effects have been studied in squid of the genus *Loligo* and in other genera that contain giant axons, all animals that inhabit a wide variety of thermal environments. By examining the axons, Rosenthal *et al.* [18,19] have determined that their electrical properties are seasonally acclimated. Action potentials have been recorded at different temperatures and compared among giant axons isolated from squids caught in May, in relatively cold waters and in August, in relatively warm waters. In a different biological context, other studies have addressed the effects of heating on conductive properties in myocardium [20]. The response of myocardial impulse propagation to hyperthermia has been quantified and the temperatures required for transient and permanent block in conduction identified [21]. In order to explain the experimental results obtained for nerves, several papers have proposed a "condenser theory" which attributes the observed initial heat not to any chemical event but rather to the free energy released in the lipid dielectric upon discharge of the membrane capacity. This energy would all be released as Joule heating of the medium upon complete discharge of the membrane capacity. During repolarization, the free energy is again stored in the membrane capacity. If the source of this energy were the thermal energy of the ions in solution there would be a corresponding cooling of the medium [7,13,16,17]. To summarize, although experimental data exist for local effects associated with heat transfer in nerves, a theoretical model coupling action potential physics with temperature variations is not addressed in the literature. Thus we have found it natural to explore modifications induced by time-varying temperature gradients, i.e., both global and local heat transfer effects in excitable tissues. Although the quantitative physiological models can differ significantly in the number and complexity of equations, it is well known that the (temperature-independent) standard FitzHugh-Nagumo (FHN) model is a good first approximation for all of them [22,23]. Consequently, in order to build a simplified model of heat transfer in excitable systems, we will take into account the global thermal effects using the theoretically fit discussed in classical HH experiments [1] in which the axon was kept at constant temperature.

We have then translated these results into FHN theory and

 ©2006 The American Physical Society

coupled them with a simplified version of Pennes' *bioheat equation* [24] by assuming time- and space-varying temperatures, which represent local effects. In particular we have been interested in obtaining two maps, one describing the propagation of the action potential and a corresponding second one showing the thermal behavior in time of the electrically stimulated tissue.

The main results of our analysis are the observation in simulations of the evolution in time of hotter spots on elongated fibers as a consequence of the Joule effect during the whole spread of an action potential pulse. Such results agree with the most credible hypothesis on heat propagation in nerve fibers, i.e., the above mentioned condenser theory. In particular, on square domains containing electric spiral waves, hotter patterns with temperature on the order of tens of μ°C appear close to the spiral's tip.

The paper is organized as follows. In Sec. II we derive generalized FHN equations including heat transfer coupling, giving the details in Appendix A. In Sec. III we perform some analytic estimates keeping the temperature constant. In Sec. IV we then pass to a numerical integration of the general equations in order to have a dynamical view of heat transfer (a dimensionless variable analysis is given in Appendix B). Finally, possible experimental implications of such a phenomenon in biological context are discussed in Sec. V.

II. HEAT TRANSFER IN THE FITZHUGH-NAGUMO MODEL

Models describing the propagation of electrical excitation waves in heart or brain tissues generally consist of two parts: a model of the cardiac or neural cell, and a model describing cellular interconnections. In general, the excitation of a cell is brought about by the change in potential across the cell membrane, due to transmembrane fluxes of various charged ions (Na^+, K^+, Ca_2^+, Cl^-, etc.) and a mathematical description of these processes is based on the following equation [25]:

$$I = C_m \frac{dV}{dt} + I_m, \tag{1}$$

where I represents the total transmembrane current, C_m is the membrane capacitance, V is the transmembrane potential, and I_m is the ionic transmembrane current. The time dependence of the excitation of a single cell in the absence of external currents is modeled by Eq. (1) with $I=0$. In order to describe wave propagation in the tissue as a whole it is instead necessary to specify the currents resulting from the intercellular coupling (I); these currents in turn are usually responsible for (spatial) variations of the transmembrane potential V, and such a behavior is well approximated by a cablelike equation. All the existing studies describing electric propagation in the giant squid axon have been performed keeping the whole axon at uniform and constant temperature via an external heat reservoir [1]. However, the current flux and subsequent voltage spread in the fiber, due to space variations of V in time, should create a heat transfer leading to a space and time dependence of T. Consequently, $T=T(t,\vec{x})$ should be inserted into the HH model equations, and these in turn should be coupled to a Fourier-type equation for the dynamical temperature spread. To accomplish this we use a modification of the well known Pennes' bioheat equation [24], originally introduced to account for possible metabolism and blood flow in a biological tissue. Assuming an electric contribution (that is, an additional heat source), Pennes' equation results in [26–28]

$$\underbrace{\nabla_i(k_{il}\nabla_l T)}_{\text{conduction}} + \underbrace{w_b c_b (T_a - T)}_{\text{perfusion}} + \underbrace{\sigma_{ik}\nabla_i V \nabla_k V + q_m}_{\text{heat sources and sinks}} = \underbrace{\rho c_p \partial_t T}_{\text{energy storage rate}}, \tag{2}$$

where $\hat{k} \equiv k_{il}$ is the thermal conductivity tensor of the tissue and T is the temperature, while w_b and c_b are the blood perfusion and heat capacity and T_a is the arterial temperature. In Eq. (2) summation on repeated indices is assumed.

For the giant squid axon modeled by HH, the perfusion term can be interpreted as the rate of heat transfer between a seawater bath around the axon having temperature T_a and the axon itself. The quantity q_m is the metabolic heat term (which accounts for production and reabsorption of heat due to effects associated with the molecular structure of the cell), ρ is the tissue density, c_p is the heat capacity of the tissue, and $\hat{\sigma} \equiv \sigma_{ik}$ is the electrical specific conductivity tensor (per unit volume), measured in S/m. Thermal unit conventions follow those of Ref. [26].

A biological medium is a conducting medium [29] in which electric current diffuses, the current vector being

$$j_i = \sigma_{ik}(\mathcal{E}^k - \delta \nabla^k T), \tag{3}$$

where $\mathcal{E}^k = -\nabla^k V$. This equation states that even in the absence of current flow, a gradient of temperature will generate an electric field (thermoelectricity). For simplicity, in the following we will neglect thermoelectricity, i.e., we assume $\delta = 0$.

Under these assumptions, the power source in the heat equation is $\vec{j}\cdot\vec{E} \equiv \sigma_{ik}\nabla_i V \nabla_k V$, i.e., the well known Joule effect. Concerning the conductivity tensor, we point out that in the existing literature, starting from the original HH papers up to more accurate analyses of the wave propagation speed [25,30,31], the conductivity is always considered temperature independent for temperature variations up to 25 °C, since this assumption is in good agreement with experiments.

However, as shown in a recent study of seasonal variations (i.e., environmental temperature variations) of conduction velocity in squid giant axons [18], resistive changes in the axon are experimentally observed. The generalized FitzHugh-Nagumo model including such heat transfer effects is shown below, while the detailed steps of its derivation are presented in Appendix A:

$$\frac{\partial i}{\partial t} = \phi(T)\left(\frac{V - V_0 - Ri}{L}\right), \tag{4}$$

$$C_m \frac{\partial V}{\partial t} - D_0 \nabla^2 V = -\left(\frac{\eta(T)}{A}\right)[F(V) + i] - I_0, \tag{5}$$

$$k_0 \nabla^2 T + \sigma_0 (\nabla V)^2 + c_* w_* (T_* - T) = \rho c_p \partial_t T. \tag{6}$$

In these equations the variable V is the action potential, i is a gating variable, and T is the temperature. The remaining quantities, discussed in Appendix A, belong to the circuit equivalent representation of the FHN model and to the heat equation properties in biological tissues. Following a standard procedure these equations can be made dimensionless. The details are listed in Appendix B, while the final equations are

$$\frac{\partial v}{\partial \tau} = \frac{1}{\chi}\{D_1 \nabla^2 v + (1 + b\Theta)[\Sigma v(1 - v)(v - \alpha) - w] - w_0\},$$

$$\frac{\partial w}{\partial \tau} = \frac{1}{\chi} 3^{\Theta} \epsilon_{21}(v - v_0 - \gamma w),$$

$$\frac{\partial \Theta}{\partial \tau} = \frac{1}{\chi}[\epsilon_{24} \nabla^2 \Theta + \epsilon_{25} \sigma_1 \nabla v \cdot \nabla v - \epsilon_{23}(\Theta - \Theta_*)]. \tag{7}$$

The quantities v and w are the dimensionless action potential and gating variable, respectively, while Θ is related to the dimensionless temperature and the variables τ and $\vec{X}$ appearing in the partial derivatives are dimensionless time and space variables. Due to the various rescalings, new constants (e.g., ϵ_{12}, etc.) are defined in Appendix B.

Limiting case of the temperature-independent FHN equations

By setting $\Theta = \Theta_* = 0$ (i.e., $T = T_* = 6.3\ ^\circ\mathrm{C}$) and $\sigma_1 = 0$, one obtains the limiting case of the temperature-independent FHN equations in standard form [32–35]. With this choice, the first and the second equations of system (7) are the original FHN equations. As shown in the following, the extended FHN model describes phenomena producing temperature excursions on the order of tens of $\mu\ ^\circ\mathrm{C}$, according to experimental data. Due to this fact, the third equation of system (7), taking into account variations of tens of $\mu\,^\circ\mathrm{C}$ around the bath temperature $T_* = 6.3\ ^\circ\mathrm{C}$, practically does not affect the electric dynamics of the model. In fact, such a small local effect of temperature does not affect the action potential and other electric properties of the medium, as discussed in detail in Sec. IV. Consequently we can state that the case $T = T_* = 6.3\ ^\circ\mathrm{C}$ in our generalized model corresponds in practice to the temperature-independent FHN model. In the next sections, we will discuss comparisons of the extended temperature-dependent FHN with the original FHN model $[\Theta = \Theta_* = 0$ (i.e., $T = T_* = 6.3\ ^\circ\mathrm{C})]$.

III. SEMIANALYTICAL RESULTS IN SIMPLE CASES

Equations (7) form a system of coupled nonlinear partial differential equations, which can essentially be studied only numerically due to its complicated form. Before doing so, we first try to clarify the role played by temperature in the dimensionless dynamics by using semiquantitative analyses. Hereafter we will assume $\chi = 1$ without any loss of generality.

For simplicity, let us consider first the zero-dimensional FHN equations, i.e., with no spatial dependence. The third equation of (7) then implies

$$\Theta(\tau) = \Theta(0) e^{-\epsilon_{23}\tau} + \Theta_*(1 - e^{-\epsilon_{23}\tau}), \tag{8}$$

which clearly shows that soon after $\tau \sim \epsilon_{32}$ the temperature approaches the limiting value: $\Theta_\infty = \Theta_*$, as expected. The remaining equations in this case are

$$\frac{\partial v}{\partial \tau} = \{[1 + b\Theta(\tau)][\Sigma v(1 - v)(v - \alpha) - w] - w_0\}$$

$$\frac{\partial w}{\partial \tau} = 3^{\Theta(\tau)} \epsilon_{21}(v - v_0 - \gamma w). \tag{9}$$

In the absence of current densities, there cannot be a Joule effect so that the initial excess heat is reabsorbed by the metabolic perfusion term. Eliminating this term, i.e., setting $\epsilon_{23} = 0$, one gets a constant solution for the temperature $\Theta(\tau) = \Theta(0)$. We note that this case corresponds to a simplified (and rough) version of the HH experiments, i.e., an axon threaded by a metallic conductor and kept at constant temperature in a thermal bath. Defining the new time coordinate $\mu = [1 + b\Theta(0)]\tau$ and the new parameter $\tilde{\epsilon} = \epsilon_{21}[1 + b\Theta(0)]^{-1}$ and assuming $w_0 = 0$ for simplicity, we reobtain the standard FHN model

$$\frac{\partial v}{\partial \mu} = [\Sigma v(1 - v)(v - \alpha) - w],$$

$$\frac{\partial w}{\partial \mu} = \tilde{\epsilon}(v - v_0 - \gamma w), \tag{10}$$

in which only the time scales and the excitability have been modified; consequently the whole dynamics is simply rescaled. In more detail, if $\Theta(0) > 0$ one has more frequent action potentials with sharpened oscillation-relaxation behavior, while if $\Theta(0) < 0$ one obtains the opposite effect, i.e., longer periods with an elongated plateau.

We can now implement wave propagation in one dimension. We assume for simplicity that $\Theta(\tau) = \Theta(0) \equiv \Theta_*$ is constant in our equations. This case is related to the HH experiments again in which the entire axon, unthreaded this time, is externally kept at constant temperature. Imposing $w = 0$ (i.e., the bistable equation limit, see [25]), $w_0 = 0$, $\epsilon_{21} = 0$, and $\sigma_1 = 0$, the system (7) reduces to the single equation

$$\frac{\partial v}{\partial \tau} = \left(D_1 \frac{\partial^2 v}{\partial X^2} + [1 + b\Theta(0)][\Sigma v(1-v)(v-\alpha)] \right), \quad (11)$$

which admits the exact traveling-wave solution

$$v = \frac{1}{2}[1 + \tanh(\kappa X + \omega \tau)] = \frac{1}{2}[1 + \tanh \kappa(X + \tilde{c}\tau)] \quad (12)$$

where

$$\kappa = \frac{1}{2}\sqrt{\frac{\Sigma[1 + b\Theta(0)]}{2D_1}}, \quad \omega = \frac{1-2\alpha}{4}\Sigma[1 + b\Theta(0)],$$

and $\tilde{c} = \omega/\kappa = (1-2\alpha)\sqrt{\Sigma D_1[1+b\Theta(0)]}/(\sqrt{2})$ is the dimensionless wave speed. Higher temperatures then induce higher propagation velocities, in agreement with experiments on solitary traveling pulses in nerve physiology experiments [1,8,25,31]. This relation will be compared below with the results obtained by numerically integrating the full system of equations for the model for general $\Theta(\tau)$.

We can now reanalyze in more detail the problem of the time- and space-dependent variations of temperature in the one-dimensional case. Introducing advanced and retarded coordinates $\xi = X + c\tau$ and $\eta = X - c\tau$, where c is a positive constant, and requiring purely advanced solutions, i.e., dependence on the variable ξ only, the system (7) becomes an ordinary autonomous system of differential equations.

One should now find the value of the constant c for given imposed boundary conditions. In the standard FHN equations one can find the (constant and unique) value of c in the traveling-pulse case by looking for the homoclinic trajectory for example, or for the periodic wave train case, which is typically used in the standard FHN theory to get the dispersion curves at fixed values of the global temperature [25]. Heat transfer effects, however, introduced in this paper, require us to take into account possible local temperature exchanges of the entire fiber with the external environment. Such a physical situation is not possible if the axon is modeled by a one-dimensional equation system. For this reason, we prefer to model the fiber as a long thin two-dimensional object, and solve the system of partial differential equations (7) using finite-element methods. In this way suitable boundary conditions for heat transfer can be imposed.

With this aim we must fix the value of the parameters first, and then set up the numerical experiments, as shown in the next section.

IV. NUMERICAL ANALYSIS AND RESULTS OF THE MODEL

The parameters of our model in Eqs. (7) must be chosen to give results comparable with experimental data, available in the literature for nerve tissues only, mainly giant axons. We started by selecting a typical choice of temperature-independent FHN parameters [32,35], i.e., $v_0 = 0$, $\alpha = 0.1$, $\epsilon_{21} = 0.005$, $\gamma = 2$, $D_1 = 1$, $\Sigma = 1$. The remaining parameters, including parameter b, related to thermal effects and discussed in the appendixes, are determined using results summarized in Refs. [36,37], in which single impulses of action potential are measured experimentally to produce 2–7 μ°C temperature spikes in cold or room-temperature mammalian nonmyelinated nerve fibers and 23 μ°C in nonmyelinated garfish olfactory nerve fibers [14]. In order to fix the dimensionless scale length, we note that for the giant squid axon action potential (see [25], p. 254) the typical length scale is on the order of $X_0 = 0.65$ cm. Using for $R_1 C_m = 10^{-4}$ s, with the chosen value of $\epsilon_{21} \equiv (R_1 C_m)/(L/R_1) = 0.005$, we have $L/R_1 \sim 0.02$ s. In this way a dimensionless time interval $\Delta\tau = 50$ corresponds to $\Delta t = 5$ ms, a typical duration for an axon action potential (see [25], p. 129, Fig. 4.7). Moreover, using typical data for brain tissue taken from [37], $k_0 \sim 0.5$ W/m K, $\rho c_p \sim 3.9 \times 10^6$ J/m^3 K, so that $k_0/\rho c_p \sim 10^{-7}$ m^2/s. It then also follows that $\epsilon_{14} = (\rho c_p/k_0)X_0^2 \sim 10^{-5}$ (see Appendix B for the definition of these parameters). The remaining parameters are ϵ_{24}, ϵ_{25}, σ_1, ϵ_{23}, Θ_*. In our dimensionless analysis, a 10 μ°C temperature variation with respect to the reference dimensionless temperature $\Theta = 0$ means a maximal excursion of $\Theta_{\max} \sim 10^{-6}$ (unmyelinated case) when a single action potential pulse will spread in the fiber. A parametric study has shown that a value around $\epsilon_{15}\sigma_1 \sim 10^{-3}$ gives such an excursion. The value of $\Theta_{\max}$ grows monotonically with σ_1 so our parameter fixing used in the rest of our paper is unambiguous. As a remark, the myelinated case would instead require $\epsilon_{15}\sigma_1 = 10^{-4}$ or less. Higher values induce higher-temperature excursions, while lower ones give the opposite effect. This is not surprising because the parameter σ_1 is associated with the resistivity in the heat equation and regulates the influx of energy. As expected, Joule heating effects generated by the passage of the action potential are extremely small. However, if a strong external electric stimulus is applied to the fiber, such a Joule effect term could produce greater effects. As previously shown the quantity ϵ_{13} determines the thermal damping length after an action potential pulse. A choice of $\epsilon_{13} = 10$ will imply a complete reabsorption of heat on the tail of the action potential. Lower values of ϵ_{13} imply longer cooling times, which are not in agreement with experiments, however. The variable Θ_* is associated with the perfusion or background initial temperature, and in our simulations will be varied for various cases. Summarizing, our choice is the following: $\epsilon_{24} \equiv \epsilon_{14}\epsilon_{21} \sim 10^{-7}$, $\epsilon_{25}\sigma_1 \equiv \epsilon_{15}\epsilon_{21}\sigma_1 \sim 5 \times 10^{-6}$, $\epsilon_{23} \equiv \epsilon_{13}\epsilon_{21} = 0.05$.

The explicit parameter choices are summarized in Table I. In more detail, we have performed a numerical analysis of the model equations in two dimensions simulating an elongated fiber and a squared domain.

A. Elongated fiber

In order to simulate an axon as an elongated fiber, we have built a domain $\mathcal{D}$ of 200×1 space units. We have then implemented heat exchanges with the boundary. Zero-flux boundary conditions have been imposed for v and w, i.e.,

$$\hat{n} \cdot \nabla v = \hat{n} \cdot \nabla w = 0, \quad \vec{X} \in \partial\mathcal{D}, \quad (13)$$

where $\hat{n}$ is the unit normal to the boundary. For the variable Θ we have instead chosen Dirichlet conditions on the boundary:

TABLE I. Values used for the analytic and numerical analyses of the model.

Parameter	Value
χ	1
D_1	1
b	0.6
Σ	1
α	0.1
γ	2
v_0	0
ϵ_{21}	0.005
ϵ_{23}	0.05
ϵ_{24}	10^{-7}
$\epsilon_{25}\sigma_1$	5×10^{-6}
Θ_*	Various choices

$$\Theta = \Theta_*, \quad \vec{X} \in \partial\mathcal{D}, \tag{14}$$

which in dimensional form means that a thermostat is assumed to be located on $\mathcal{D}$. The initial data are

$$v(0,\vec{X}) = w(0,\vec{X}) = 0, \quad \Theta(0,\vec{X}) = \Theta_*. \tag{15}$$

The action potential is initiated by a stimulus located at one extreme of the fiber, with a smooth Gaussian profile centered on it and damped in time, i.e.,

$$w_0 = e^{-f(X-X_c)^2 - g\tau^2}, \tag{16}$$

with $f=1$, $X_c=100$, and $g=2$. Comsol MULTIPHYSICS [38] finite-element procedures, based on sufficiently fine quadratic Lagrange elements, have been adopted in union with a direct solver (UMFPACK). The results can be summarized as follows.

1. Detection of thermal and electrical response

Figure 1 shows both the dimensionless action potential and the temperature as functions of τ, measured in the center of the fiber, in the case of $T_*=6.3$ °C. As mentioned before, this situation considering temperature to be constant gives the standard FHN electrical theory. Due to heat coupling, a temperature gradient is associated with action potential propagation. As expected, the heat production and the following reabsorption are in phase with the action potential, in agreement with the experiments [7,13–15,39]. The maximum value of Θ is of the order of 10^{-6}, which corresponds approximately to 10 μ°C. This means that the parameter estimation is correct and in agreement with experiments on real nonmyelinated nerve fibers [7,17].

2. Local effects of temperature on excitability parameter

It is important now to estimate the modifications induced by a time-varying temperature on the electric parameters of the model. Introducing the temperature-dependent quantities $\epsilon_{21}(\Theta)=\epsilon_{21}3^{\Theta}$, it is interesting to study the behavior of the quantity

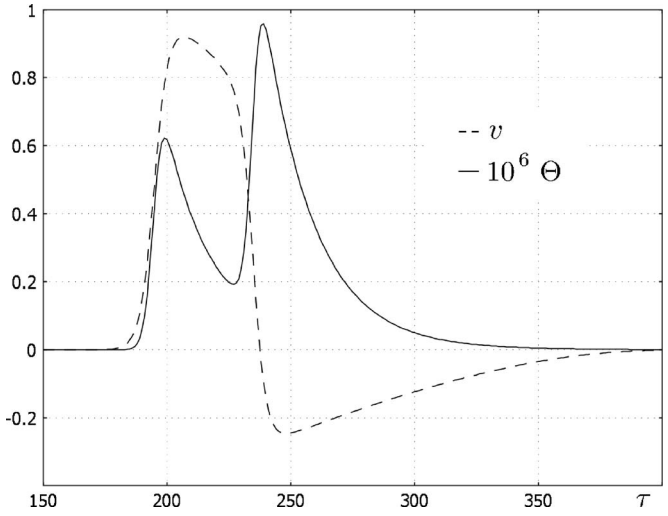

FIG. 1. Superimposed plots of the dimensionless action potential v and temperature Θ as functions of dimensionless time τ taken in the center of the fiber, in the case of $T_*=6.3$ °C ($\Theta_*=0$).

$$\Delta\epsilon_{21}/\epsilon_{21} = \frac{\epsilon_{21}(\Theta_*) - \epsilon_{21}(\Theta)}{\epsilon_{21}(\Theta_*)} = 1 - 3^{\Theta-\Theta_*}, \tag{17}$$

which might be considered as representing the relative variation of the FHN excitability after an action potential passage with respect to the constant-temperature situation.

Figure 2 shows $\Delta\epsilon_{21}/\epsilon_{21}$ in the case $T_*=6.3$ °C ($\Theta_*=0$), as a function of the dimensionless time τ. This parameter is almost unchanged with respect to the temperature-independent FHN equations; hence, the passage of an action potential pulse is a purely local effect and in practice does not affect the electrical dynamics. On the other hand, on changing the global temperature Θ_* (the thermostat) the parameter $\epsilon_{21}(\Theta)$ is noticeably affected, although $\Delta\epsilon_{21}/\epsilon_{21}$ is not, due to the modest variations for Θ, always on the order of 10^{-6}.

3. Global effects of temperature on action potential

The effect of temperature on the action potential produced by a single current pulse is studied by setting the thermostat

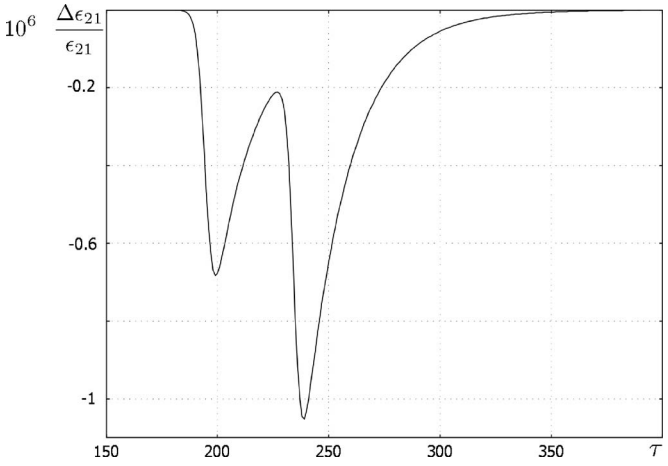

FIG. 2. Evolution in time of $(\Delta\epsilon_{21})/(\epsilon_{21})$ at the point (0, 0) in the case $T_*=6.3$ °C ($\Theta_*=0$).

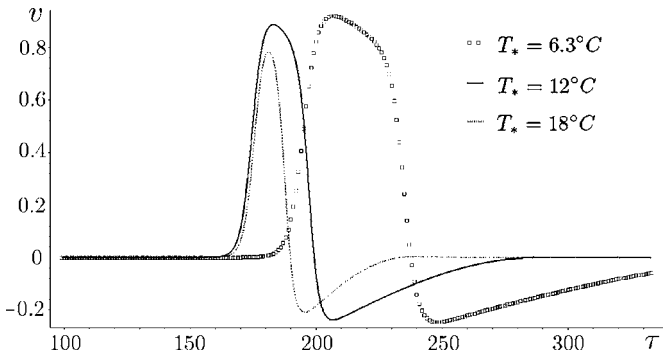

FIG. 3. Plot of the action potential v vs τ, taken in the center of the fiber, superimposed for the cases $T_*=6.3$, 12, and 18 °C. As expected, low temperatures induce larger action potential durations, while higher ones make the signal profile narrower in time and faster.

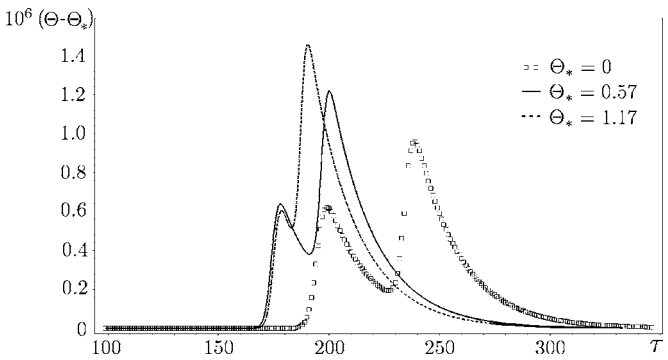

FIG. 4. Plot of $\Theta-\Theta_*$ vs τ, taken in the center of the fiber, superimposed for the cases $\Theta_*=(0,0.57,1.17)$ equivalent to $T_*=(6.3,12,18)$ °C.

at different values of temperature. Four simulations have been performed corresponding to the values $T_*=(6.3,12,18,19)$ °C, equivalent to $\Theta_*=(0,0.57,1.17,1.27)$.

In Fig. 3 we have taken the dimensionless action potential at the center of the fiber and superimposed the curves for the cases $T_*=6.3$ (standard FHN model), 12, and 18 °C. The case $T_*=19$ °C is absent due to a conduction block which does not allow the action potential to arrive at the center of the fiber, as explained below. As expected, at low temperature the spike of the action potential has a larger duration, in particular in its declining phase. On raising the temperature, the spike becomes smaller in time, because the signal has traveled faster due to high-temperature effects. In this case the action potential is diminished also in amplitude. These results are qualitatively in good agreement with the original experimental work of Hodgkin and Katz [6] and with our semianalytical estimates. Figure 3 in fact reproduces the experimental Figs. 3 and 4 of their analysis for temperatures only up to $T_*=18$ °C. While our model predicts conduction blocks for greater values of $T_*>18$ °C, experimental results do not show these phenomena unless temperatures reach values up to 35–40 °C [6]. This limit of our model for higher temperatures has the following causes.

(i) The poor physiological meaning of the FHN electrical model: On implementing the more realistic HH model, the results will have a better quantitative meaning and interpretation.

(ii) The quantity Q_{10} (see Appendix A). It is well known [1,6] in fact that Q_{10} can be assumed constant in a certain range of temperatures only. Higher temperatures require a change for the value of this constant which regulates the dynamics of ion channels, appropriate to the new temperature range. Consequently, modifying the value of Q_{10}, we could reach higher temperatures, although for the aim of the present paper we will limit our analysis to temperatures smaller than 20 °C.

4. Temperature-amplitude relation

Experimentally [6] at $T=5$ °C the corresponding action potential amplitude $V_{\max}=108.5$ mV, while at $T=18.5$ °C the action potential amplitude is $V_{\max}=99$ mV. Consequently, one has the ratio $V_{\max}(T=18.5\ ^\circ\mathrm{C})/V_{\max}(T=5\ ^\circ\mathrm{C})\sim 0.91$, while similarly using our simplified model we get $v_{\max}(T=18\ ^\circ\mathrm{C})/v_{\max}(T=6.3\ ^\circ\mathrm{C})\sim 0.87$.

5. The effect of temperature on action potential duration and shape

Experimentally [6], at $T=18.5$ °C the corresponding action potential duration (APD) $t\sim 0.8$ ms while at $T=5$ °C one has $t\sim 3.6$ ms. The ratio of $t_{\mathrm{APD}}(T=18.5\ ^\circ\mathrm{C})/t_{\mathrm{APD}}(T=5\ ^\circ\mathrm{C})\sim 0.22$, while using our simplified model (dimensionless units) $t_{\mathrm{APD}}(T=18\ ^\circ\mathrm{C})/t_{\mathrm{APD}}(T=6.3\ ^\circ\mathrm{C})\sim 0.39$.

Concerning the effect of temperature on rise of the action potential, in our model upstroke velocities depend on temperature. The values $(dV/dt)_{\max}(T=6.3\ ^\circ\mathrm{C})=0.08$ (FHN standard), $(dV/dt)_{\max}(T=12\ ^\circ\mathrm{C})=0.10$, $(dV/dt)_{\max}(T=18\ ^\circ\mathrm{C})=0.11$ show that global temperatures affect action potential properties too.

6. Heat release and reabsorption

In Fig. 4 we have plotted $\Theta-\Theta_*$ versus τ, taken in the center of the fiber, superimposed for the cases $T_*=6.3$ (standard FHN model), 12, and 18 °C. As expected a traveling pulse of action potential, in the case of a thermostat temperature T_* in the range $T_*=6.3-18$ °C, produces a corresponding temperature variation of 10–15 μK.

7. Space and time evolution of action potential spread

Figure 5 shows for temperature values $T_*=6.3$ (standard FHN model), 12, 18, and 19 °C the development in space and time (dimensionless units) of the action potential v, measured on a line parallel to the long side and passing in the middle of the fiber. As expected, in the case of lower temperature $T_*=6.3$ °C (standard FHN model), the thickness of the action potential (evaluated by a vertical section and corresponding to its duration), is larger and the speed is slower in comparison with the other three cases.

The action potential thickness evaluated by a horizontal section and corresponding to its wavelength shows a decreasing wavelength as the temperature increases.

Higher temperatures $T_*=12$, 18, and 19 °C induce a thinner spike and lower the slope of the line representing the

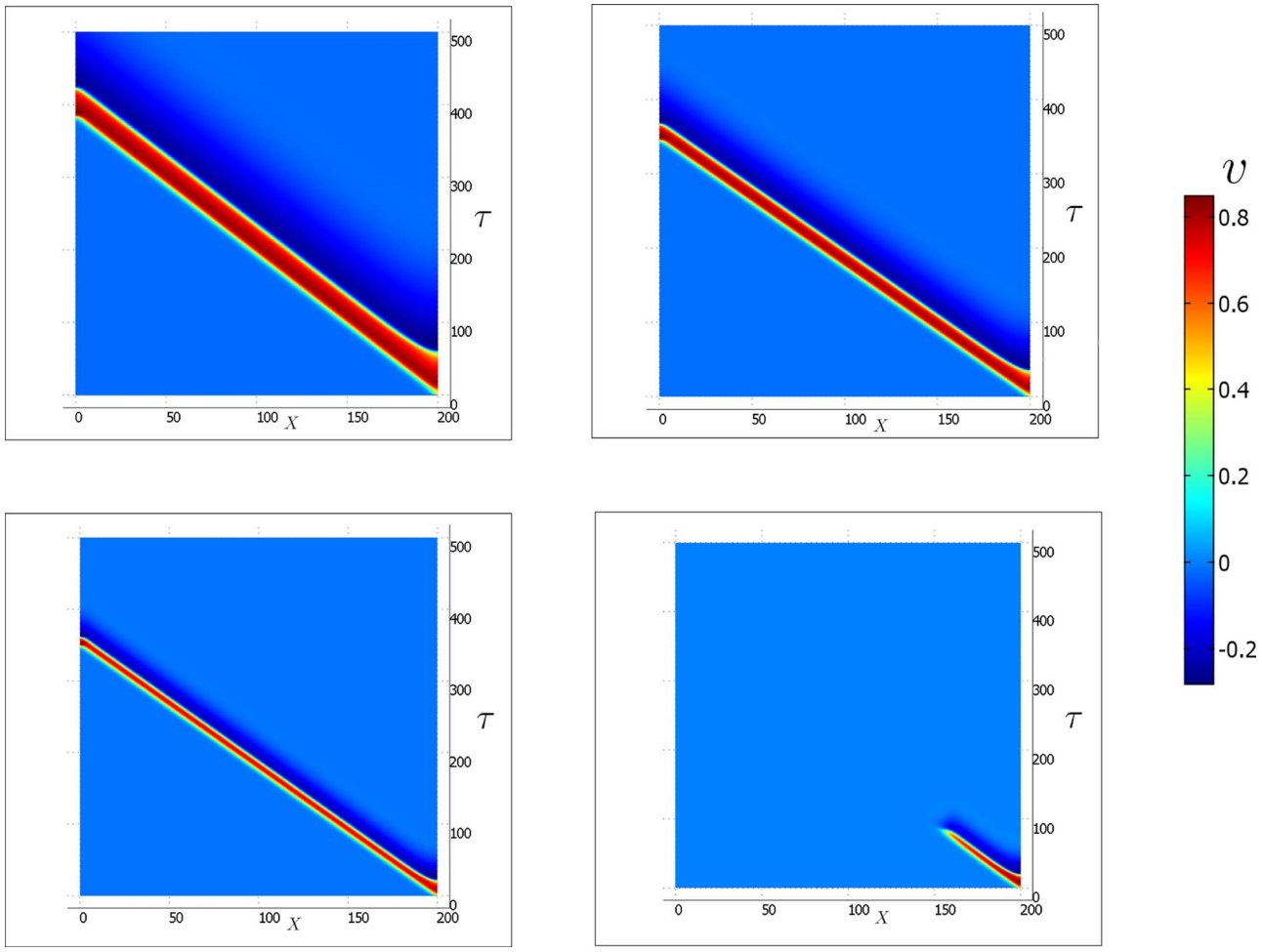

FIG. 5. (Color online) Plots in the τ-X plane of a traveling pulse v for $T_*=6.3$ and 12 °C (top left and right figures) and for $T_*=18$ and 19 °C (bottom left and right figures). The signal is measured on a line parallel to the long sides and passing in the middle of the fiber. Notice the increasing speed conduction with temperature, the action potential contraction, and, in the hottest case, the presence of a conduction block.

traveling pulse in the plane X-τ, which implies increased conduction velocities according to Chapman's analysis [8]. The last case of $T_*=19$ °C is remarkable in that the conduction failed ("heat block") after a few dimensionless time units. As discussed above, this is also expected from experiments [6,21].

8. Conduction velocity

Figure 6 shows the conduction velocity at different temperatures (dimensionless units) for the analytic solution in the bistable equation limit, contrasted with the same quantity obtained from the numerical integration of the exact model. The trend is similar, showing that a higher background temperature induces higher conduction speed for a traveling action potential pulse. This model, whose parameters have been calibrated for an elongated nerve fiber, can now be applied to a domain that is not elongated, i.e., to a square region representing a patch of neural tissue.

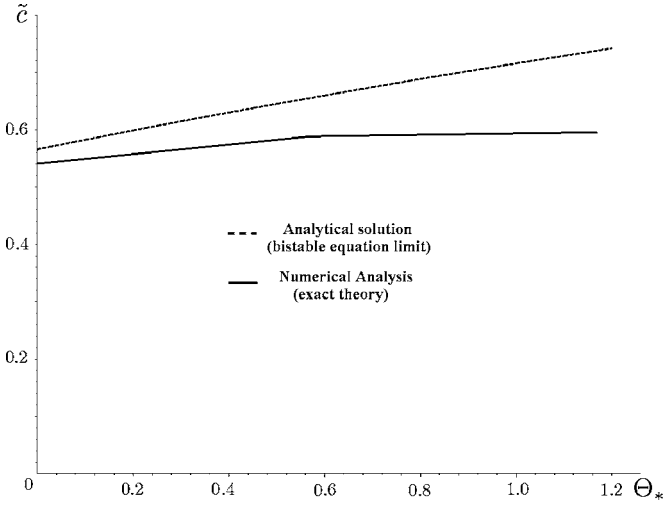

FIG. 6. The dimensionless velocity at different dimensionless temperatures for the analytic solution in the bistable equation limit contrasted with the same quantity obtained from the numerical integration of the exact model.

B. Square domain

In our generalized FHN model we have analyzed the dynamics of electrical and thermal activities in a two-

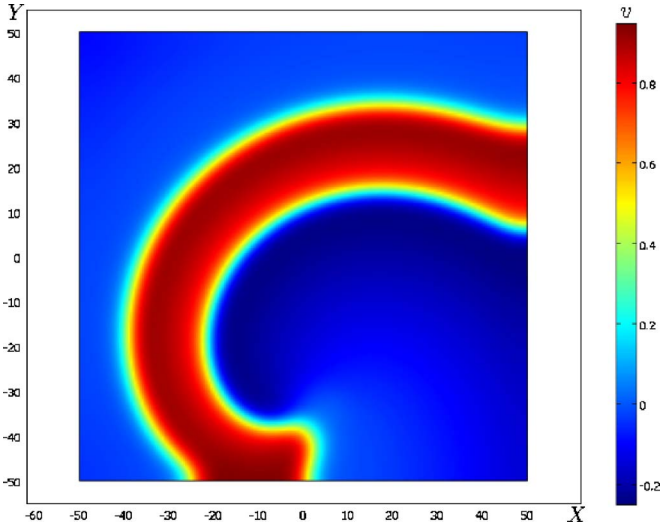

FIG. 7. (Color online) Dimensionless action potential v map at $\tau=500$.

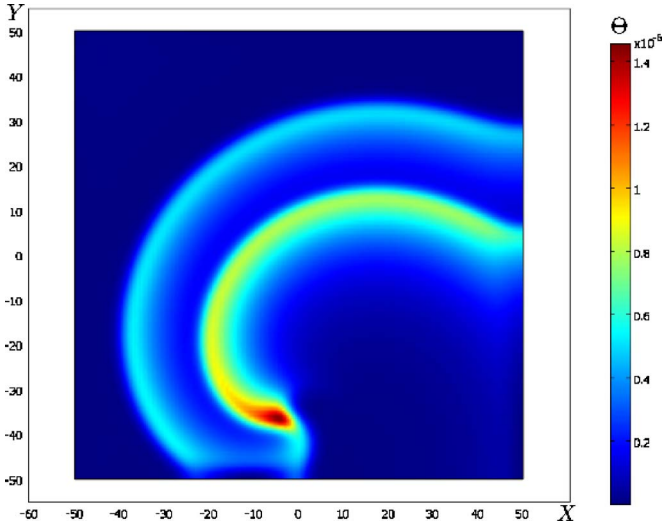

FIG. 8. (Color online) Dimensionless temperature Θ map at $\tau=500$.

dimensional square domain. In detail, we have performed a simulation on a square of 100×100 dimensionless space units, centered at the origin. Boundary conditions in this case have been chosen to be zero flux for v, w, and Θ to avoid boundary effect contamination in the dynamics. The initial data for w and v have been chosen to initiate a spiral wave, i.e., $v=0.8$ in the rectangle $X>0$ and $Y>5$ while $w=0.2$ in the rectangle $X>0$ and $Y<-5$. The dimensionless temperature at the initial time has been chosen to be $\Theta=0$. This means $T_*=T_0=6.3$ °C (i.e., $\Theta_*=0$). In principle one should have defined different constant temperatures on the activated and refractory rectangles, respectively. We have neglected this modification of the initial data, assuming that shortly after the beginning of the simulation, such a heat differential would have been totally reabsorbed by the medium, resulting essentially in a short-lived effect not relevant for the code evolution. This assumption will be justified later, when we will discuss the spiral's tip trajectory in the temperature domain. Quadratic Lagrange finite elements are used again to numerically solve the problem. The mesh used was 100×100 squared elements with $\Delta X=1$. Regarding time stepping, we have used a fine adaptive algorithm of Comsol MULTIPHYSICS software, such that the maximum time step is $\Delta\tau=0.15$. The numerical integration was stopped after 3000τ time units. With these choices, the magnitude of the maximum violations of the zero-flux boundary conditions is $\sim10^{-5}$. The map of voltage v at time $\tau=500$ is shown in Fig. 7 with the characteristic spiral pattern. Figure 8 shows the dimensionless temperature Θ at time $\tau=500$: here the electrical spiral pattern generates a spiral temperature wave due to the Joule effect. Figure 9 shows the same plot as Fig. 8 but with the isovoltage lines and the trajectory of the spiral's tip in the interval $\tau=360-500$ superimposed. We note that the regions in which the gradient of v is steeper appear to be hotter (a consequence of the Joule term), while the spiral's tip is contained in the hottest area (around 15 μ°C). It is remarkable that the heat has been reabsorbed quite rapidly and there is no hot trail in coincidence with the tip's trajectory. Moreover, the tip's trajectory is essentially the same as in the temperature-independent FHN model, due to the fact that temperature excursions of some tens of μ°C have almost no influence on the electric dynamics of the system. Clearly in the case of different initial data and boundary conditions such that there could be temperature variations of some °C, the spiral tip's trajectory will be modified noticeably, although this analysis will not be addressed here and will be left for future work. Finally, Fig. 10 shows the evolution in time τ of v and Θ at the point $(X,Y)=(-40,0)$. Again as expected the heat release and reabsorption are totally in phase with the action potential, as occurs in the previously discussed axon simulations. However, a modulation effect in the temperature is present and this fact can be ex-

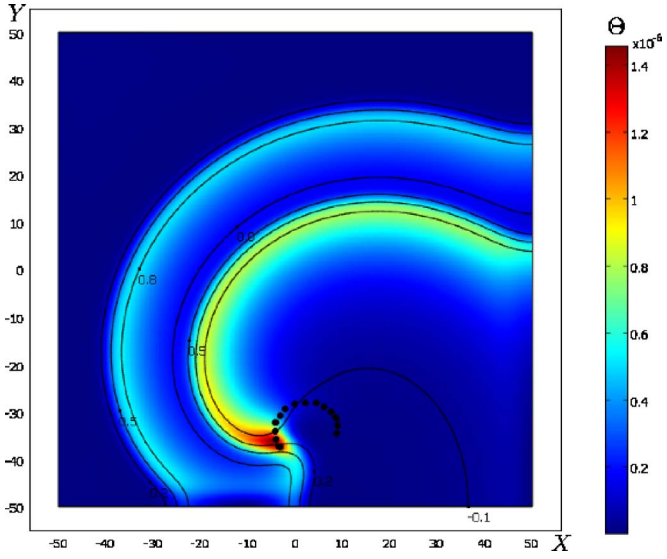

FIG. 9. (Color online) Dimensionless thermal Θ map at $\tau=500$ superimposed by the isovoltage v lines and the trajectory of the spiral's tip in the interval $\tau=360-500$. In hotter areas the electric gradient changes noticeably and a hotter spot is present (14 μ°C) close to the spiral's tip. The colored legend is relative to the value of Θ.

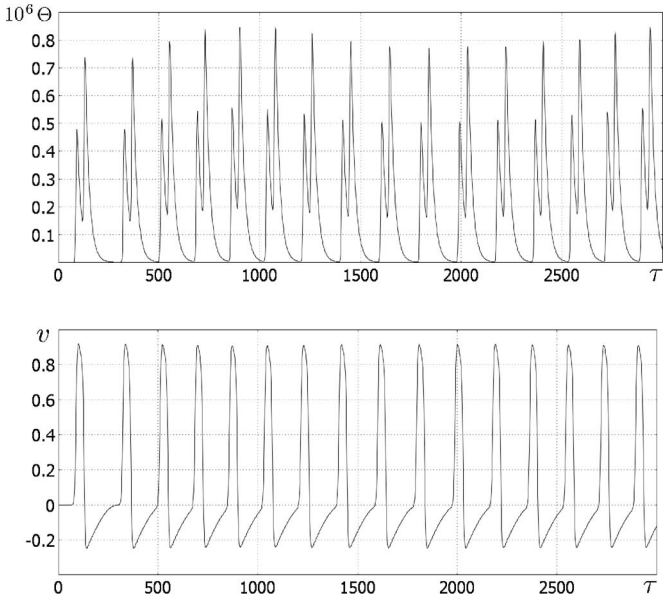

FIG. 10. Evolution in time of dimensionless temperature Θ and the action potential v shown at the point $(X,Y)=(-40,0)$ due to the spiral wave's dynamics.

plained by Fig. 11, in which we have shown the spiral's tip trajectory which manifests a meandering such that the spiral tip (the hotter area) can be far from or close to the observation point P.

V. CONCLUSIONS

We have discussed a wide set of experimental results, focused on temperature effects in excitable biological tissues.

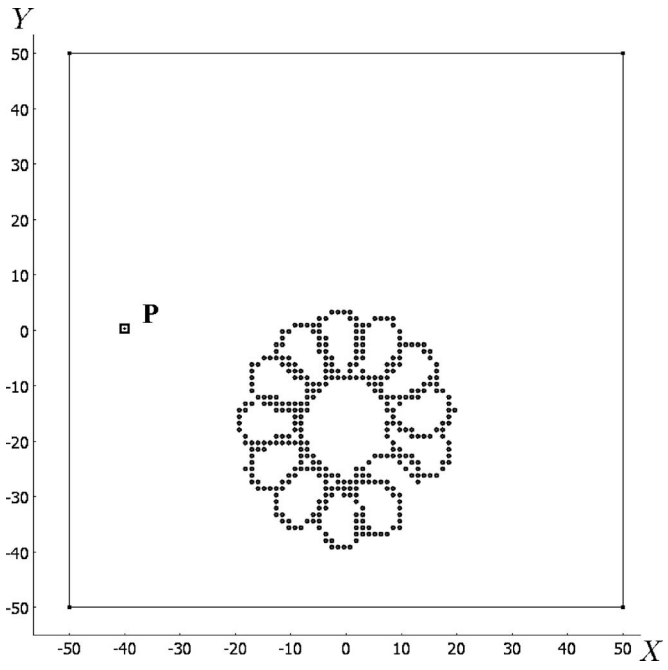

FIG. 11. Spiral tip trajectory and observation point P located at $(X,Y)=(-40,0)$.

In the framework of mathematical models and in particular in Hodgkin-Huxley's theory the temperature is assumed to affect the kinetics of channels and currents and can have a dramatic effect on the kinetics of gating. Ideally, then, it should be accounted for in a model by incorporation of the Q_{10} experimentally determined scaling factor. However, heat transfer effects traditionally have been neglected. In this paper, we have built a generalized FitzHugh-Nagumo model which includes dynamical heat transfer in tissues, described by a bioheat equation and resulting in a thermoelectric coupling. The characteristics of the model agree with the most credible hypothesis on heat propagation in nerve fibers, the condenser theory. Calibrating model parameters to match typical experimental data, we have performed a series of simulations for a two-dimensional elongated fiber and for a square domain, qualitatively representing an axon and a neural tissue, respectively, although different choices of parameters should describe other excitable tissues described by FHN equations, like cardiac cells for example. The model reproduces many experimental features such as (1) the action potential duration shortening and amplitude decrease as temperature is raised; (2) the conduction velocity increase with temperature; (3) the existence of conduction blocks at sufficiently high temperatures, and (4) the heat release and reabsorption in phase with the action potential. In two dimensions, simulations suggest that electric waves generate a spiraling pattern in the temperature domain with hotter spots around the spiral's tip, having temperature variations of tens of μ°C. This may give a possible way to physically identify the spiral's tip. Thermal detectors constructed by using a thin film of synthetic pyroelectric material, polyvinylidene fluoride (PVDF) are typical tools for analyzing such tiny heat processes in stimulated nonmyelinated nerve fibers. The response of such detectors is very fast and the time for half-maximum deflection is of the order of 1 ms [15]. These tools could be used for analyzing such heat transients predicted by this generalized model.

APPENDIX A: DERIVATION OF THE EQUATIONS FOR THE MODEL

The classical one-dimensional HH equations [1,25] for the electric propagation in the giant squid axon, externally kept at uniform constant temperature T, are given by

$$C_m\frac{\partial V}{\partial t}=\frac{p}{2r}\frac{\partial^2 V}{\partial x^2}+\eta(T)[g_{\mathrm{Na}}m^3h(V_{\mathrm{Na}}-V)+g_{\mathrm{K}}n^4(V_{\mathrm{K}}-V)+g_l(V_l-V)]+I_{\mathrm{app}},$$

$$\frac{\partial j}{\partial t}=\phi(T)[\alpha_j(V)(1-j)-\beta_j(V)j], \tag{A1}$$

where $j=m,h,n$ and $\alpha_j(V),\beta_j(V)$ are specific functions proposed by HH (listed, e.g., in [25], p. 127) and the numerical values of the membrane capacitance C_m, the channel conductances g_{Na}, g_{K}, g_l, the axon's radius p, and the resistivity of the intracellular space r can also be found in [25]. The temperature-dependent factor $\phi(T)=Q_{10}^{(T-T_0)/Q}$ in the second

equation was given by HH with $T_0=6.3$ °C and $Q=10$ °C, $Q_{10}=3$ while the factor $\eta(T)=A[1+B(T-T_0)]$ in the first equation was introduced by Moore [40] and subsequently reanalyzed by FitzHugh [11,22]. A is the (constant) ratio between ionic conductances of the axon at 6.3 °C while B determines the rate of change of conductance with temperature. The values of A and B vary considerably from axon to axon; here we fix their values following FitzHugh and Cole [41], i.e., $A\sim 1.14$ and $B\sim 0.06$ °C^{-1}. In this paper we have been concerned with an approximation of the HH model, i.e., the FitzHugh-Nagumo theory, studying the coupling of the associated equations with the bioheat equation. Following Keener and Sneyd's monograph [25] this simplified model can be obtained easily using a simplified scheme for the cell membrane as an electric circuit. We assume that the cell consists of a capacitor, representing the membrane capacitance, a nonlinear current-voltage device for the (fast) current, and a resistor, inductor, and battery in series for a (slow) recovery current [25]. Using Kirchhoff's laws, we get

$$I_m = F(V) + i + I_0, \tag{A2}$$

where I_0 is an applied external current, i is the current through the resistor-inductor, and $F(V)$, left generic for the moment, is a cubic function of the potential having three real roots located at $V=0$, αV_1, and V_1 with $0<\alpha<1$ and the smallest and the largest ones corresponding to stable solutions of

$$\frac{dV}{dt} = -F(V). \tag{A3}$$

We take the passive resistance of the nonlinear element to be $R_1=1/F'(0)$. By direct evaluation, Eq. (1) becomes

$$\nabla\cdot(\hat{D}\,\nabla V) = C_m\frac{\partial V}{\partial t} + F(V) + i + I_0. \tag{A4}$$

This equation is coupled to

$$\frac{\partial i}{\partial t} = \frac{V - V_0 - Ri}{L}, \tag{A5}$$

where $\hat{D}=D_{ik}$ is the conductivity tensor (measured in S m^2), V is the membrane potential, V_0 is a potential gain across a battery, and R and L are the resistance and the inductance of the membrane. Typically in cable equation theory, quantities (capacity, inductance, currents, etc.) are measured per unit area. For convenience we restore proper units by multiplying cable equation by a common area term. The coupled equations (A4) and (A5) are often considered sufficient to describe the basic propagation of electric signals over a physiological excitable tissue, neglecting heating effects. One can derive a temperature-dependent FHN model as follows:

$$\frac{\partial i}{\partial t} = \phi(T)\left(\frac{V - V_0 - Ri}{L}\right),$$

$$C_m\frac{\partial V}{\partial t} - \nabla\cdot(\hat{D}\,\nabla V) = -\left(\frac{\eta(T)}{A}\right)[F(V)+i] - I_0, \tag{A6}$$

where the temperature-dependent factors are chosen exactly as in the temperature-dependent HH relations. Equations (A6) will be a prototype for general temperature-dependent excitable biological tissues. They must be coupled to a modified Pennes' equation

$$\nabla_i(k_{il}\nabla_l T) + \sigma_{ik}\nabla_i V\nabla_k V + c_* w_*(T_* - T) = \rho c_p \partial_t T, \tag{A7}$$

where the term $c_*w_*(T_*-T)$ accounts for both axon perfusion and possible metabolic effects, considered linear in the temperature for simplicity.

In fact it is experimentally known that such effects tend to redistribute heat in the medium immediately after an action potential pulse has spread [7,12–15], allowing the fiber to come back to the "initial temperature" T_*. In general T_* should depend on space and time, i.e., $T_*=T_*(t,\vec{x})$, although in this paper we assumed for the sake of simplicity T_* =const. We remark that this temperature is in principle different from the "reference temperature" T_0 entering $\phi(T)$ and $\eta(T)$. We have assumed for simplicity temperature-independent conductivity tensors and for a similar reason we adopt a temperature-independent $\hat{k}$ to avoid self-diffusion effects [42]. Moreover, we have limited our consideration here to homogeneous and isotropic tissues, which means in Cartesian coordinates $\hat{\sigma}\equiv\sigma_0\delta_{ik}$, $\hat{D}\equiv D_0\delta_{ik}$, and $\hat{k}\equiv k_0\delta_{ik}$, with σ_0, D_0, and k_0 constants.

APPENDIX B: DIMENSIONLESS ANALYSIS

Equations (4)–(6) can be put into a simpler form by introducing standard dimensionless variables.

Let us denote the typical action potential and resistance scale values by $V_s=V_1$ and $R_s=R_1$, respectively. It follows that $i_s=V_1/R_1$ is a typical current scale value. It is natural to introduce the following dimensionless variables:

$$v(t,\vec{x}) = \frac{V(t,\vec{x})}{V_1}, \quad w(t,\vec{x}) = \frac{R_1}{V_1}i(t,\vec{x}), \tag{B1}$$

where $\vec{x}=(x,y,z)$ denotes the actual position vector in space; analogously, the following dimensionless quantities can be introduced:

$$v_0 = \frac{V_0}{V_1}, \quad w_0 = \frac{R_1}{V_1}I_0, \quad \gamma = \frac{R}{R_1}, \tag{B2}$$

together with

$$f(v) = -\frac{R_1}{V_1}F(V_1 v) \equiv \Sigma v(v-\alpha)(1-v), \tag{B3}$$

where Σ is a free parameter for the model. Because of the simplification arising limiting our attention to the case of homogeneous and isotropic tissues, it is clear that we may have a common length scale factor L_s for all three spatial axes. Let $L_s=X_0$ be such a common value so that

$$X = \frac{x}{X_0}, \quad Y = \frac{y}{X_0}, \quad Z = \frac{z}{X_0} \tag{B4}$$

are dimensionless quantities. To introduce a time scale factor, from Eqs. (4) and (5) we are faced instead with two possible choices,

$$t_s^{(1)} = \frac{L}{R_1}, \quad t_s^{(2)} = R_1 C_m, \tag{B5}$$

so that the quantity

$$\epsilon_{21} = \frac{t_s^{(2)}}{t_s^{(1)}} = \frac{R_1^2 C_m}{L} \tag{B6}$$

is dimensionless. We introduce the notation

$$\epsilon_{ij} = \frac{t_s^{(i)}}{t_s^{(j)}}, \quad \epsilon_{ji} = \epsilon_{ij}^{-1} \tag{B7}$$

used below. Let us select $t_s^{(1)}$ as the time scale, i.e., introduce the dimensionless time variable:

$$\theta = \frac{t}{t_s^{(1)}} = \frac{R_1}{L} t. \tag{B8}$$

The next step is that of introducing scales for the electric (specific) conductivity and diffusivity. From dimensional analysis, a typical scale for diffusivity is $D_s = X_0^2/R_1$; hence, we will denote by D_1 the dimensionless quantity associated with D_0:

$$D_0 \frac{R_1}{X_0^2} = D_1. \tag{B9}$$

Analogously, a typical scale for conductivity is $\sigma_s = 1/(X_0 R_1)$, so that σ_1 is the natural dimensionless quantity associated with σ_0:

$$\sigma_0 R_1 X_0 = \sigma_1. \tag{B10}$$

Finally, the same model equations suggest a way to introduce scales for the temperature. In fact, we have various possibilities:

$$T_s^{(1)} = T_0, \quad T_s^{(2)} = T_*, \quad T_s^{(3)} = Q. \tag{B11}$$

We find it convenient to use $T_s^{(3)} = Q$ as a scale for the temperature. Thus, we introduce

$$\Theta(t, \vec{x}) = \frac{T(t, \vec{x}) - T_0}{Q} \tag{B12}$$

as the dimensionless variable associated with the temperature. Actually, from Eqs. (4)–(6) other time scale quantities can be defined:

$$t_s^{(3)} = \frac{\rho c_p}{w_* c_*}, \quad t_s^{(4)} = \frac{\rho c_p X_0^2}{k_0}, \quad t_s^{(5)} = \frac{\rho X_0^3 c_p Q}{V_1^2/R_1}, \tag{B13}$$

so that other dimensionless ratios, used below, can be formed:

$$\epsilon_{13} = \frac{w_* c_* L}{\rho c_p R_1}, \quad \epsilon_{14} = \frac{k_0 L}{R_1 \rho c_p X_0^2}, \quad \epsilon_{15} = \frac{V_1^2 L}{\rho c_p Q X_0^3 R_1^2},$$

$$\epsilon_{23} = \frac{R_1 C_m w_* c_*}{\rho c_p}, \quad \epsilon_{24} = \frac{k_0 R_1 C_m}{\rho c_p X_0^2}, \quad \epsilon_{25} = \frac{V_1^2 C_m}{\rho c_p Q X_0^3}. \tag{B14}$$

Furthermore we define

$$b = BQ = 0.6 \tag{B15}$$

using values previously discussed in the HH case. Finally, letting $\Theta_* = \Theta|_{T=T_*}$, we obtain the (dimensionless) quantity

$$\Theta_* = \frac{T_* - T_0}{Q}. \tag{B16}$$

The dimensionless heat-transfer–FHN coupled equations then take the form

$$\epsilon_{21} \frac{\partial v}{\partial \theta} = D_1 \nabla^2 v + (1 + b\Theta)[\Sigma v(1 - v)(v - \alpha) - w] - w_0,$$

$$\frac{\partial w}{\partial \theta} = 3^{\Theta}(v - v_0 - \gamma w),$$

$$\frac{\partial \Theta}{\partial \theta} = \epsilon_{14} \nabla^2 \Theta + \epsilon_{15} \sigma_1 \nabla v \cdot \nabla v - \epsilon_{13}(\Theta - \Theta_*), \tag{B17}$$

where here the Laplace and gradient operators are referred to the (Cartesian) dimensionless variables X, Y, Z. Rescaling time by $\tau = (\chi/t_s^{(2)})t \equiv (\chi/\epsilon_{21})\theta$, one obtains an alternative dimensionless form, precisely Eqs. (7).

[1] A. L. Hodgkin and A. F. Huxley, J. Physiol. (London) **117**, 500 (1952).

[2] A. L. Hodgkin, *The Conduction of the Nervous Impulse* (Liverpool University Press, Liverpool, U.K., 1964).

[3] J. Cronin, *Mathematical Aspects of Hodgkin-Huxley Neural Theory* (Cambridge University Press, Cambridge, U.K., 1987).

[4] A. T. Winfree, *The Geometry of Biological Time* (Springer, Berlin, 2000).

[5] J. Bernstein, Pfluegers Arch. Gesamte Physiol. Menschen Tiere **92**, 521 (1902).

[6] A. L. Hodgkin and B. Katz, J. Physiol. (London) **109**, 240 (1949).

[7] B. C. Abbott, A. V. Hill, and J. V. Howarth, Proc. R. Soc. London, Ser. B **148**, 149 (1958).

[8] R. A. Chapman, Nature (London) **213**, 1143 (1967).

[9] R. A. Sjodin and L. J. Mullins, J. Gen. Physiol. **42**, 39 (1958).

[10] R. Guttman, J. Gen. Physiol. **49**, 1007 (1966).

[11] R. FitzHugh, J. Gen. Physiol. **49**, 989 (1966).

[12] J. V. Howarth, J. M. Ritchie, and D. Stagg, Proc. R. Soc. London, Ser. B **205**, 149 (1958).

[13] T. Heimburg and A. D. Jackson, Proc. Natl. Acad. Sci. U.S.A. **102**, 9790 (2005).
[14] I. Tasaki, K. Kusano, and P. M. Byrne, Biophys. J. **55**, 1033 (1989).
[15] I. Tasaki and P. M. Byrne, Jpn. J. Physiol. **42**, 805 (1992).
[16] J. V. Howarth, R. D. Keynes, and J. M. Ritchie, J. Physiol. (London) **194**, 745 (1968).
[17] J. M. Ritchie and R. D. Keynes, Q. Rev. Biophys. **392**, 451 (1985).
[18] J. J. C. Rosenthal and F. Bezanilla, Biol. Bull. **199**, 135 (2000).
[19] J. J. C. Rosenthal and F. Bezanilla, J. Exp. Biol. **205**, 1819 (2002).
[20] C. Mc. C. Brooks, W. V. MacFarlane, and J. O. Pinkston, Am. J. Physiol. **171**, 711 (1952).
[21] T. A. Simmers, J. M. De Bakker, F. H. Wittkampf, and R. N. Hauer, J. Am. Coll. Cardiol. **25**, 1457 (1995).
[22] R. FitzHugh, Biophys. J. **1**, 445 (1961).
[23] J. Nagumo, S. Arimoto, and S. Yoshizawa, Proc. IRE **50**, 2061 (1962).
[24] H. H. Pennes, J. Appl. Physiol. **1**, 93 (1948).
[25] J. Keener and J. Sneyd, *Mathematical Physiology* (Springer, Berlin, 1998).
[26] R. V. Davalos, B. Rubinsky, and L. M. Mir, Bioelectrochemistry **61**, 99 (2003).
[27] S. Tungjitkusolmun, S. T. Staelin, D. Haemmerich, J. Tsai, H. Cao, J. G. Webster, F. T. Lee, Jr., D. M. Mahvi, and V. R. Vorperian, IEEE Trans. Biomed. Eng. **49**, 3 (2002).
[28] K. R. Diller, J. W. Valvano, and J. A. Pearce, in *Handbook of Thermal Engineering*, edited by F. Kreith (CRC Press, Boca Raton, FL, 1999).
[29] E. M. Lifshitz, L. D. Landau, and L. P. Pitaevskii, *Electrodynamics of Continuous Media*, Course of Theoretical Physics Vol. 8, 2nd ed. (Butterworth-Heinemann, London, 1984).
[30] R. N. Miller and J. Rinzel, Biophys. J. **34**, 227 (1981).
[31] C. B. Muratov, Biophys. J. **79**, 2893 (2000).
[32] F. H. Fenton, E. M. Cherry, H. M. Hastings, and S. J. Evans, BioSystems **64**, 73 (2002).
[33] S. Takagi, A. Pumir, L. Kramer, and V. Krinsky, Phys. Rev. Lett. **90**, 124101 (2003).
[34] A. Pumir and V. Krinsky, J. Theor. Biol. **199**, 311 (1999).
[35] D. Brown, J. Feng, and S. Feerick, Phys. Rev. Lett. **82**, 4731 (1999).
[36] C. Koch, *Biophysics of Computation: Information Processing in Single Neurons* (Oxford University Press, Oxford, 2005).
[37] R. A. Freitas, *Nanomedicine, Vol. I: Basic Capabilities* (Landes Bioscience, Georgetown, TX 1999).
[38] Computer code MULTIPHYSICS (COMSOL, 1997–2006).
[39] I. Tasaki, Jpn. J. Physiol. **49**, 125 (1999).
[40] J. W. Moore, Fed. Proc. **17**, 113 (1958).
[41] R. FitzHugh and K. S. Cole, Biophys. J. **4**, 257 (1964).
[42] J. Crank, *The Mathematics of Diffusion*, 2nd ed. (Oxford University Press, New York, 1980).